Fibre-Multi-Object Spectrograph (FMOS) for Subaru Telescope

Masahiko Kimura[a], Toshinori Maihara[a], Kouji Ohta[a], Fumihide Iwamuro[a], Shigeru Eto[a], Masafumi Iino[a], Daisaku Mochida[a], Takanori Shima[a], Hiroshi Karoji[b], Jun'ichi Noumaru[b], Masayuki Akiyama[b], Jurek Brzeski[c], Peter Gillingham[c], Anna Moore[c], Greg Smith[c], Gavin B. Dalton[d], Ian Tosh[e], Graham Murray[f], David Robertson[f], Naoyuki Tamura[f]

[a] Kyoto University, Kyoto, Japan, [b] Subaru Telescope, Hilo, Hawaii, USA, [c] Anglo-Australian Observatory, Epping, Australia, [d] University of Oxford, Oxford, UK, [e] Rutherford Appleton Lab, Oxon, UK, [f] University of Durham, Durham, UK,

ABSTRACT

The Fibre Multi-Object Spectrograph (FMOS) is a second-generation common-use instrument of the Subaru telescope. Under an international collaboration scheme of Japan, UK, and Australia, a realistic design of FMOS has already been completed, and the fabrications of hardware components have been in progress. We present the overall design details together with the special features of FMOS subsystems, such as the prime focus corrector, the prime focus mechanical unit including fibre positioners, and the near-infrared spectrograph, etc.

Keywords: Multi-object spectrograph, large telescope, near-infrared, OH suppression, optical fibre, VPH grating

1. INTRODUCTION

FMOS exploits the F/2 prime focus of the 8.2 m Subaru telescope with a new three element corrector for near-infrared (NIR) bands, which provides us with a field of view as wide as 30′ in diameter. To acquire 400 objects at the prime focus, we have developed a unique fibre positioning system together with an OH-airglow suppressed spectrograph systems. It is expected to explore various scientific frontiers from nearby substellar objects to the large scale structure of the high-redshift universe.[7] The instrument is being built under the Japan-UK-Australia international collaboration scheme.

FMOS consists of a number of subsystems; Prime Focus Unit (PFU), fibre bundle/connectors, two spectrographs, and two spectrograph cameras. PFU comprises a fibre-positioning system, an NIR-optimized corrector lens and a mechanical structure. The fibre-positioning system (which we call "Echidna", an mammal in Australia with movable spines on his back) adopts piezo driven actuators to position each of the 400 fibres. The corrector lens system is made of three spherical elements and has no ADC. These systems will be reported separately in this volume. Each spectrograph is designed to get spectra of 200 objects fed by fibre bundles from a PFU. The optical and mechanical design of the spectrographs will be reported in the later section. Figure 1 shows a bird's eye view of the whole FMOS system.

In this volume we present a number of the associated works of the FMOS project, which are papers presented by Gillingham et al.,2002[4] and Moore et al.,2002[9] on the fibre positioner, Murray et al.,2002[11] on the fibre connector, and Lewis et al.,2002[6] on the IR-spectrograph.

Further author information: (Send correspondence to M.K.)
M.K.: E-mail: kimura@kusastro.kyoto-u.ac.jp, Telephone: +81 75 753 3908
Address: Kitashirakawa, Sakyo-ku, Kyoto, 606-8502, Japan

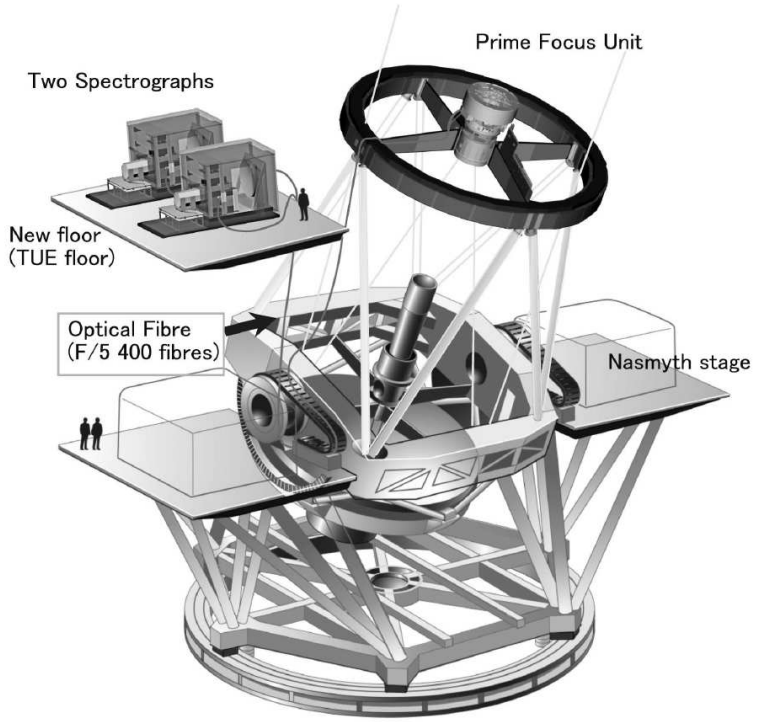

Figure 1. The whole view of FMOS. The fibre positioning system is located in the center section (PFU) at the top of the telescope, and two IR-spectrographs are placed on the upper floor of the dome.

2. PRIME FOCUS UNIT (PFU)

2.1. PFU Assembly

The prime focus unit (PFU) dedicated to FMOS has two remotely controllable adjustment mechanisms: one is a focus adjustment mechanism that rectifies the focal length to compensate possible change due to temperature variation, and the other is an offset mechanism of the corrector assembly as a whole that compensates a lateral shift of optical axis, which may be due to the deviation from the Serrier truss principle. The former mechanism is connected to an instrument rotator, and hold the instrument bay which carries the Echidna, the focal plane imager, and the Shack-Hartmann system. The latter mechanism is mounted on a flange, which interfaces the PFU assembly to the inner topring of telescope.

The present PFU designed for FMOS has a versatile nature in that a different instrument, such as a wide field near-infrared camera, could also be accommodated. The sketch of conceptual design for PFU is shown in Figure 2.

2.2. Prime Focus Corrector

Subaru telescope has currently commissioned the sophisticated prime focus corrector optimized for the optical wavelength, which has been used in the wide-field camera mode with the instrument called "Suprime-Cam".[5] Since the present corrector only covers optical wavelength, it is necessary for FMOS to have a new corrector optimized in the near infrared.[4] Figure 3 show a 3D virtual view of a new corrector system consisting of three elements made of the single glass BSM51Y. At the bottom of Figure 3, the spot diagram of optical design is shown. The 80 % encircled energy diameter is $0''.7$ enev at the periphery, sufficient for fibres with core diameter of 100 μm to acquire objects.

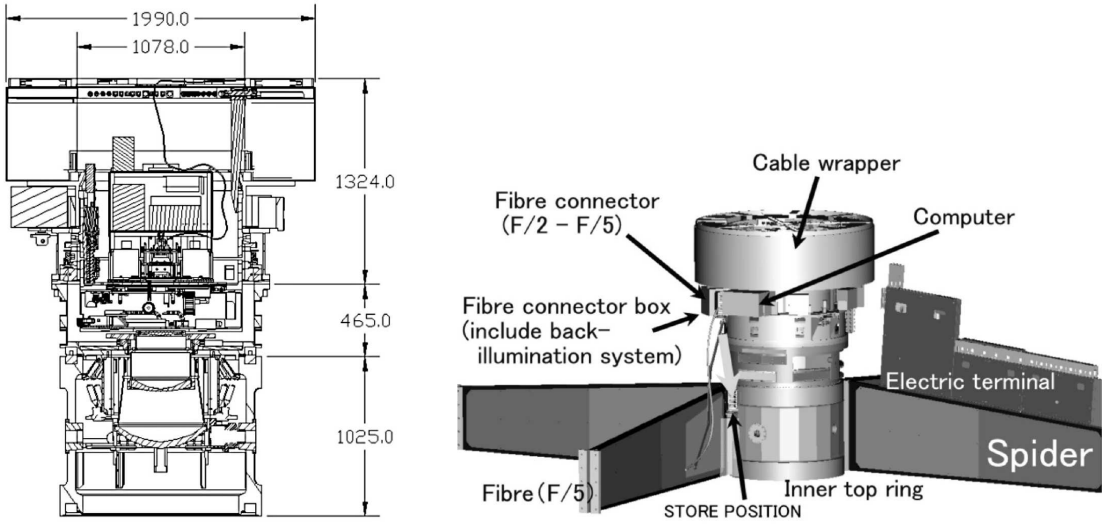

Figure 2. The cross sectional view of PFU (left), and 3D virtual view of PFU (right) as attached to the prime focus section of the Subaru telescope. When FMOS is removed from the telescope, the fibre bundle will be stored in a side of the spider.

The blur circles of images due to atmospheric dispersion for the wavelength spanning from 0.9 to 1.8 μm are estimated to be $0''.1$ and $0''.3$ in diameter at zenith distances of 30° and 60°, respectively. In the periphery of the field of view, the blurs increase to $0''.3$ and $0''.5$ due to the chromatic distortion at the respective positions. Nevertheless the fibre entrance diameter is much larger than the size of the dispersion, so that in our corrector system for FMOS we have eliminated the atmospheric dispersion corrector (ADC).

Figure 3. The optical and mechanical design of the prime focus corrector optics. The spot diagram of the corrector at zenith distance of 0 degree at wavelength 0.9, 1.37, and 1.8μm is shown at bottom. The circles represent a diameter of 100 μm, and RMS spot sizes and 80% encircled energy diameters are listed in μm. Note that 83 μm corresponds to $1''$.

2.3. Fibre Positioner and Focal Plane Imager

The area of prime focus (about 150 mm in diameter) is too tight to use a conventional positioner using magnetic buttons as employed, for example, by 2dF/AAT. Therefore we have to develop a new fibre positioning system[3,4,9] capable of positioning up to 400 fibres in a narrow area of the prime focus.

The positioner components (which we call "spines") are based on the so-called tube piezo actuators, capable of tilting the spine by electric pulse trains of a saw-tooth shape. Each spine has length of 160mm from the tip of the fibre to the pivot ball, and covers circular area of 7mm ($1'.4$) in radius by tilting up to 2.5 degree. The optical loss caused by the tilt to the incident beam is less than 10% even at the maximum tilt. The overall view of the fibre positioning system is shown in Figure 4 (left). The actual positions of the tips of the fibres are monitored by the focal plane imager CCD system to measure the displacement of each fibres, as shown in Figure 4 (right). The imaging system called Focal Plane Imager (FPI) has two cameras; the sky camera is for the sky view and the spine camera for the fibre tip view. The sky camera checks direction of the telescope referring to the position of a number of bright stars. The spine camera covers the whole area of the fibre tips in conjunction with a XY-stage, which carries the camera, and it provides information of positional errors on the each spine. After comparing the position of each fibre with the pre-determined position, the positioner driver will take actions to make the difference null. It has been confirmed in the test that the positional accuracy of fibre tips less than 10μm is achieved with 5 iterations. The configuration time of 400 fibres will be less than 10

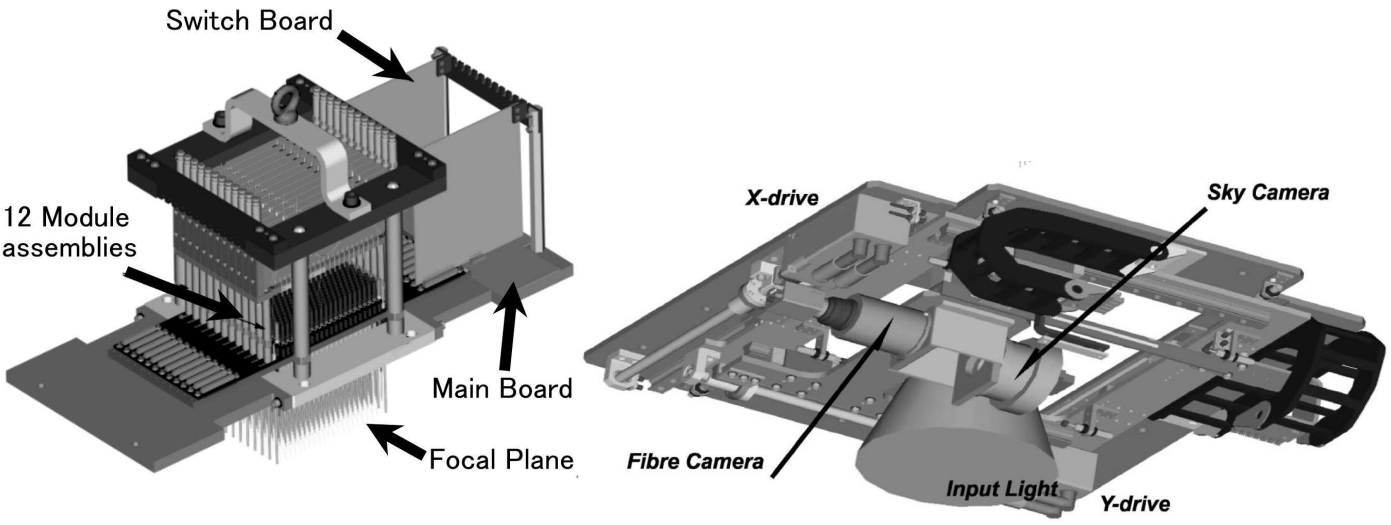

Figure 4. Whole view of fibre positioner(left) and Focal Plane Imager(right)

.

2.4. Fibres and Fibre Connectors

We have adopted fibres with a core-diameter of 100μm, which corresponds to $1''.2$ on the sky (see Figure 3). Since the F-ratio is approximately F/2 with the new prime focus corrector, we need a fibre-fibre connector converting from F/2 to F/5 so as to prevent the focal ration degradation and match it to the input focal ratio of the NIR spectrograph. The connector is based on the Selfoc lens coupler, and the expected coupling efficiency is about 95% over the wavelength range from 0.9 to 1.8 μm. The layout of the system is shown in Figure 5.

Furthermore, it is necessary for fibre connectors[11] to be equipped with a back-illumination device which is used to check a fibre position on the focal plane. The back-illumination device introduces coded light to each fibre for accurate identification and the spine camera of FPI makes use of this light in measuring contemporary positional errors at each fibres.

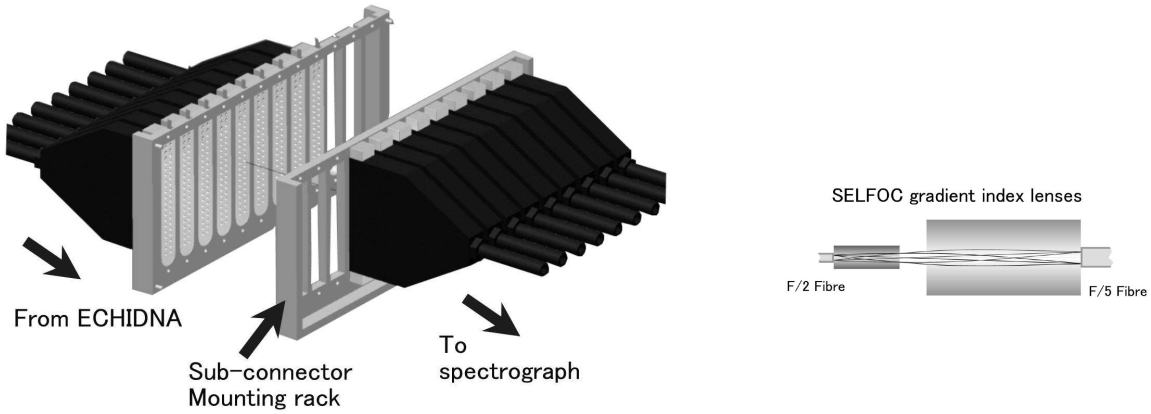

Figure 5. The F/2 - F/5 fibre connector: The mechanical structure is shown at the left. Twelve modules made of 40 fibre couplers are stacked as one unit. A close up view of the connector (right) shows the optical layout of the connector.

3. NEAR-INFRARED SPECTROGRAPH

The FMOS IR-Spectrograph has four main features. Figure 6 shows the whole view of infrared spectrograph.

- It covers a wavelength range from 0.9 to 1.8 μm.
- The spectrograph has two spectral resolution modes; With the low resolution mode (R=500) wavelength range 0.9 - 1.8 μm is covered by one exposure, and with the high resolution mode (R=2200) the full wavelength range by four exposures at four camera positions.
- Bright OH-airglow lines are suppressed by using blacked stripes on the mask mirror in the pre-optics system.
- Thermal emission from optical components is a major noise source. Therefore we put the whole spectrograph optics within a large refrigerator thereby keeping the temperature at about -50 C°.

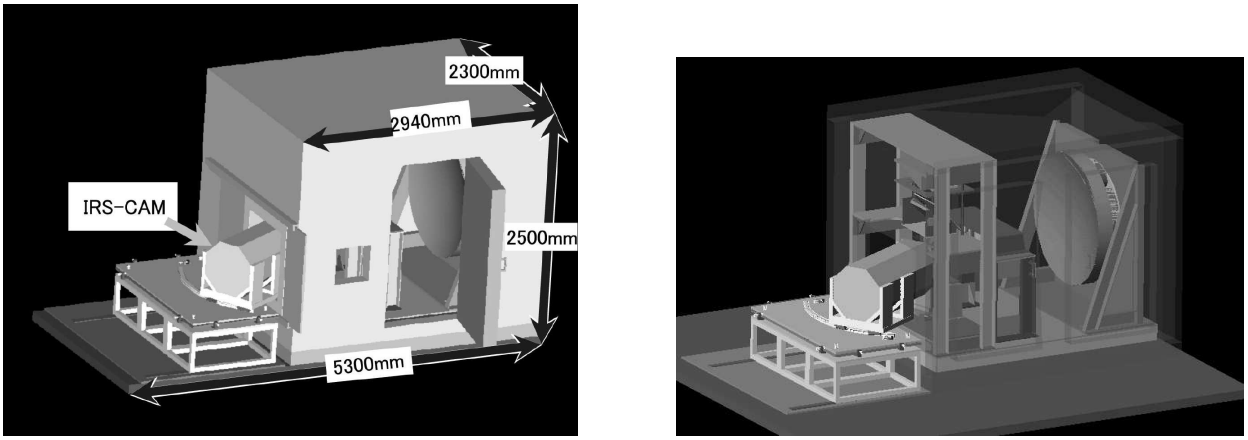

Figure 6. 3D-view of the spectrograph layout. The whole structure, except for the IR camera, is put in the refrigerator box. The left figure shows an over view with the door opened, while the right figure demonstrates the internal optical system through the wall.

3.1. OH-airglow suppression pre-optics

This portion is designed to disperse the light and to remove OH-airglow emission lines by the mask mirror (a kind of spectroscopic filter), whose basic optical layout was reported in the first paper.[7] In Figure 7, we present the final optical design, and Table 1 lists specifications of each component. The row of 200 fibre outlets acts as a long slit of the spectrograph, which is placed in the central gap of the mask mirror.

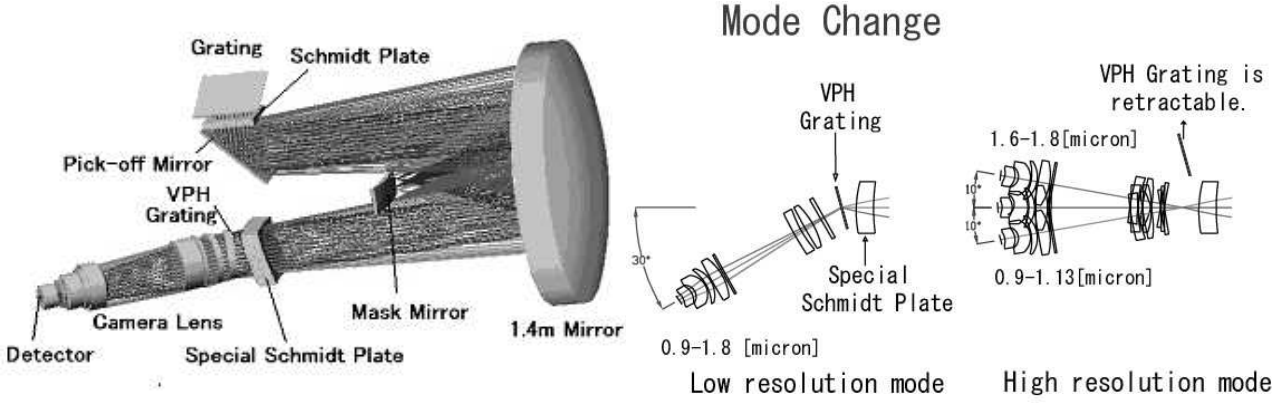

Figure 7. 3D-view of the OH-suppression spectrograph optics. The beam train presentation of the OH suppressor optics (left), and the method of changing two modes between low- and high- resolution observation (right). The whole structure, except for the IR camera, is put in the refrigerator.

The setting angle of each fibre varies in the slit assembly so as to produce a virtual pupil on the first high-resolution grating, as well as on the VPH grating. In this optical layout we need uncomfortably large camera lenses. Therefore we looked for a modified solution, in which the second pupil is produced near the front camera lens, rather than on the VPH grating. Finally it was found that the position of the second pupil could be shifted to the position between the VPH grating and the first camera lens, if we modified the second Schmidt plate to a meniscus shape (which we call the "special Schmidt plate").

3.2. Special Schmidt Plate

The special Schmidt plate has a meniscus form, each surface of which is aspheric. The use of this special Schmidt plate, we have made an outstanding improvement in terms of image quality in the entire field, and also have reduced diameters of the camera lenses. However, the shape of special Schmidt plate is a complex form, and we cannot rely on conventional methods to fabricate it.

The actual fabrication of the special Schmidt plate is underway. We came to a conclusion that using a new method called "ELID (ELectrolytic In-process Dressing)" is useful for us to produce this plate. The ELID grinding method is a unique method, which was developed in the Institute of Physical and Chemical Research (RIKEN) in Japan. The maximum error of surface figure over the carved region is expected to be less than 3 μm and the surface roughness is in the order of a few nm. We may require a polishing process by lapping after the grinding to remove the remaining small roughness and irregularity.

3.3. Volume Phase Holographic Grating

FMOS use a VPH grating. Figure 9 demonstrates an equi-efficiency contour map of a VPH grating on the wavelength - incident angle or diffraction angle plane optimized for FMOS. By virtue of this diagram it is understood that we can take advantage of higher efficiency domain as incidence angle changes along with wavelength. The VPH grating in the FMOS spectrograph optics serves as an inverse-dispersive element to reduce the spectral resolution of the original beam. With this inverse-disperser, we expect that the whole

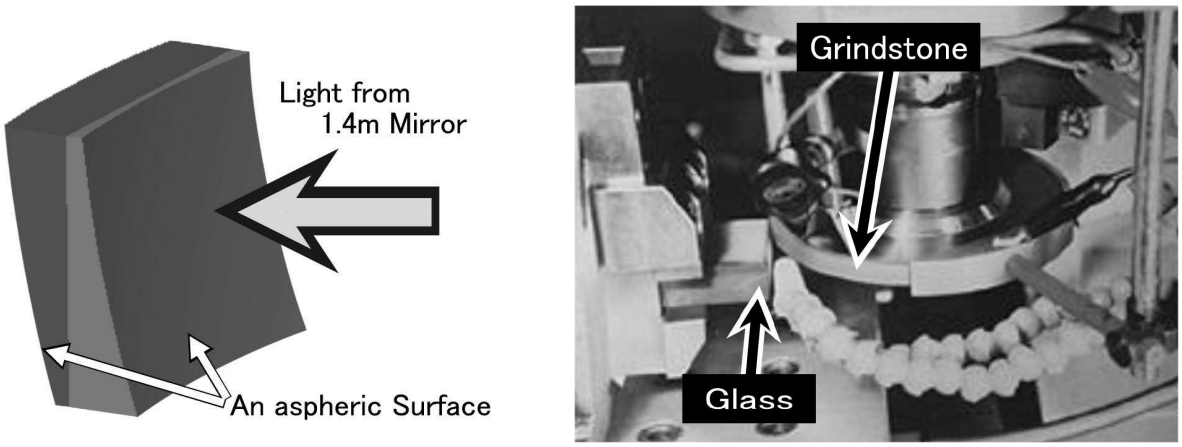

Figure 8. An illustration of special Schmidt plate (left figure) and the ELID machine (right). Refer to information at, http://www.elid.ne.jp/main.html. Both surfaces, front and back, are carved and polished independently on different pieces of silica glass. Two pieces are adhered to make a single meniscus shape.

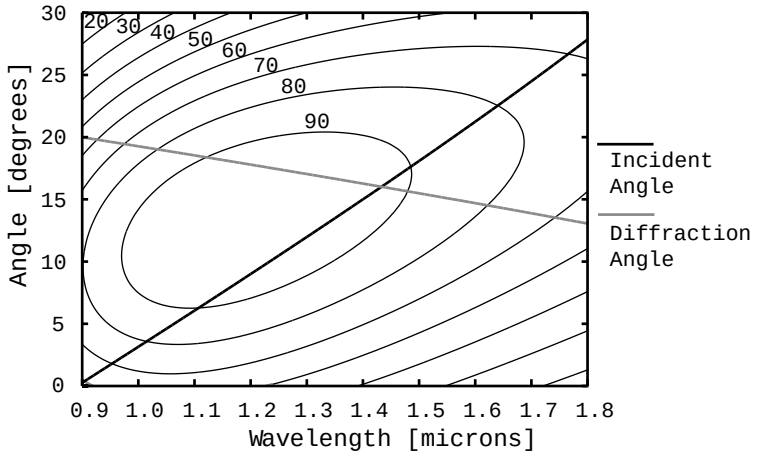

Figure 9. The equi-efficiency contour on the wavelength vs. incident angle in unit of % calculated with the Kogelnik model. The solid line represents the relation of incident angle vs. wavelength in the FMOS configuration. The thin line shows the corresponding diffraction angle.

wavelength region will be covered with efficiencies no less than 50%, while the maximum efficiency is more than 90 %.

Although the VPH grating has higher throughput over a wide wavelength range, it uses unusual material called dichromated gelatine(DCG). Since the behavior of DCG in the cold environment has not been tested extensively, we have to check the characteristics in the cold environment. The results of a preliminary test of a VPH grating at low temperatures (about -50 C°) is shown in Figure 10, using a spectrophotometer specially designed for tests of dispersive elements.

It is interesting to see that the relataive efficiency drops down to 92 % during the initial cooling phase, but it recovers after about 24 hours while the temperature is still kept low at about -50 C°. The right panel of Figure 10 shows the results of several cycles of cooling test. It seems that there is no significant efficiency change by cooling.

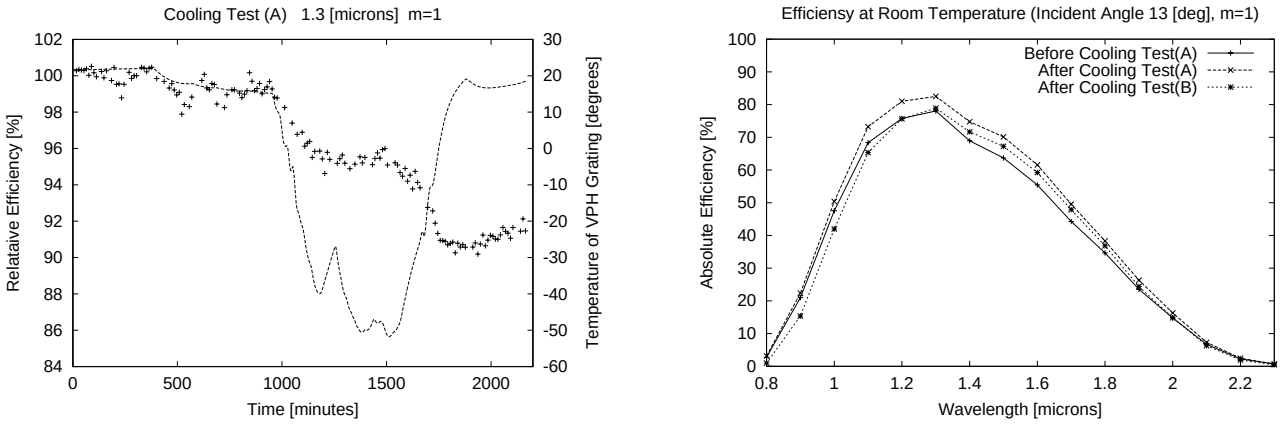

Figure 10. Results of a cool down test of VPH grating. The test sample is from KOSI, with a size of 75 × 75 mm. Left panel shows a relative efficiency by the dot, and the temperature history by the solid line. Right panel shows the efficiency change with cold cycle, (A) represents efficiency just before and after the first cycle, and (B) represents efficiency after a few days.

3.4. IR-Camera

The layout of the IR camera optics is presented in Figure 11. All of the lenses are made by fused silica. A thermal cut filter is placed between the 2nd and 3rd lens, with a cut-off wavelength of 1.8 μm. The optics is capable of reproducing spectra of 200 objects over the entire spectral range (0.9 - 1.8 μm) in the low resolution mode onto a HAWAII 2 array. When the VPH grating is taken away from the beam, we can get images of high resolution mode.

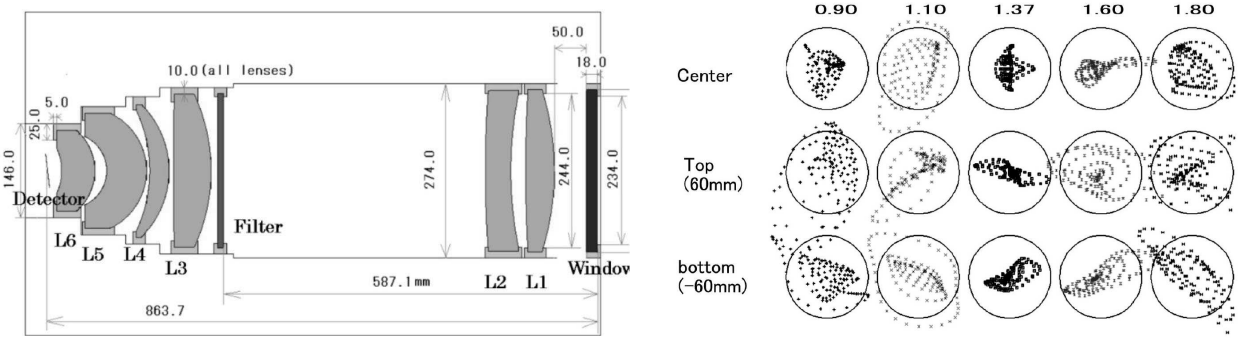

Figure 11. The Optical layout of dewar(left) and the spot diagrams on the detector(right). The circles represent a diameter of 40 μm at the wavelength 0.9, 1.10, 1.37, 1.60 and 1.80 μm, and the fibre slit places the center of mask mirror, which height is 120mm.

The spot diagram of focal plane images of the IR camera in the low-resolution mode is shown in Figure 11. The spot sizes are smaller than 2×2 pixels on the detector with the 80 % encircled energy of 40 μm in diameter. The average image size is 25 μm RMS at 0.9 μm in diameter, which corresponds to nominal spectral resolution of about 500 and 2200 in the low- and high-resolution modes, respectively. Note that the focal plane of camera optics is slightly tilted in order to compensate the chromatic effect, and moreover the tilt angle is remotely switched according to bands selected.

No.	Component	Material	Curvature[a] (mm)	Thickness (mm)	Size (mm)
1	Fibre Slit Assembly	fibre	–	–	120 long
2	Collimator	mirror	1940.0	165.0	1400ϕ
3	Fold Mirror	mirror	–	35.0	350×375
4	Schmidt Plate	silica	–	33.0	600×600
			R[c]		–
5	Grating	mirror	–	35.0	240×310
	(500/mm, $\theta_b = 20.08°$)				
10	Mask Mirror	mirror	992.76	951.02	164×520
12	Special Schmidt Plate	silica	R[d]	88.50	209×262
			R[e]	111.74	209×262
13	VPH Grating	BK7	–	10	265ϕ
	(372/mm, $\theta_{\text{deflection}} = 15.2°$)[b]			100	
14	Window	silica	–	18	240ϕ
15	Lens 1	silica	429.92	45	250ϕ
		–	-2247.27		–
16	Lens 2	silica	-604.20	40.00	246ϕ
		–	-1747.65		–
17	Filter	silica	–	9.87	234ϕ
18	Lens 3	silica	284.69	59.22	234ϕ
		–	-5118.37		–
19	Lens 4	silica	146.29	30.37	202ϕ
		–	222.43		–
20	Lens 5	silica	100.12	62.58	170ϕ
		–	59.14		–
21	Lens 6	silica	83.97	52.20	52ϕ
		–	87.92		–
22	Detector				

[a] An radius of curvature for each component is indicated.
[b] The angle by which the light axis deflects after passing VPH.
[c] Asphere parameter : a2=-2.1535e-5, a4=6.7894e-11, a6=3.6067e-17
[d] Asphere parameter : a2= 5.3612e-4, a4=5.3327e-11, a6=-1.027e-15
[e] Asphere parameter : a2= 5.3835e-4, a4=-4.857e-12, a6=-9.459e-16

Table 1. Optical Components of IR spectrograph

3.5. Mechanical Structure

In the NIR, the thermal emission from the instrument itself is one of the most significant noises. Therefore it is required to suppress the thermal emission noise to achieve high S/N. In the optical design of FMOS spectrograph, the IR camera is basically a wide-field imager, which receives collimated beams incoming from diverse directions depending on wavelength. In consequence, it suffers from thermal emission of the OH-suppression pre-optics at an ambient temperature even if the cryogenic camera optics has a built-in thermal-cut filter. This is an essential difference with the Subaru OHS, currently being operated as one of the common-use instruments[2,10] because the Subaru OHS has a slit image in front of the camera optics after OH-airglow lines has been removed. To reduce the thermal emission of the pre-optics, we have to cool down the whole instrument by a very large refrigerator. We calculated the number of thermal photons within the wavelength range up to 1.8 μm in 1000 sec (typical exposure time for FMOS) per pixel, and we found that the temperature of the pre-optics is required to be less than -50 C°.

Figure 6 and Figure 12 show the overview of the pre-optics and dewar. Since it is quite difficult to operate the camera dewar at low temperature because the camera is accompanied by electrical and mechanical components which are not adaptable to low temperature, we have to put the dewar outside the refrigerator.

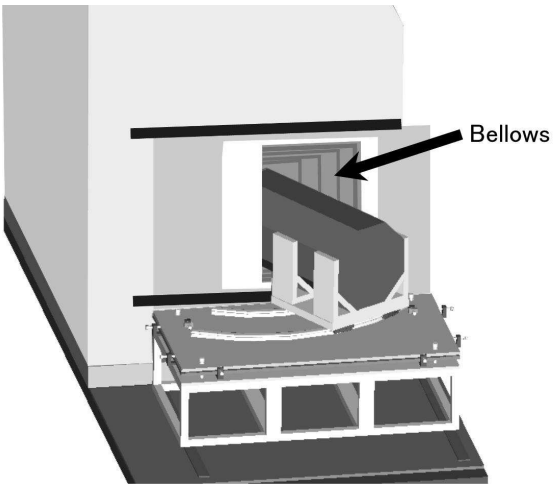

Figure 12. The figure is shown for the low resolution mode, and we use an adiabatic bellows.

As described in section 3.1, the dewar is supposed to be set at four different positions within ± 10 degree from the optical axis of the spectrograph, according to selection of sub-bands in the high resolution mode. On the other hand, the dewar has to be set at about + 30 degree from the optical axis in the low resolution mode. (c.f. Figure 12). To cope with such mechanical requirements, we have employed an adiabatic bellows which connecting the head of the dewar to the movable wall of refrigerator.

4. SUMMARY

Design details of FMOS are presented which meet the target specifications such as the multiplicity of measurements of about 400 within a 30 arcmin field, the simultaneous coverage of the whole range from 0.9 to 1.8 μm, and the OH-airglow suppression capability. We have shown completed designs of each subsystem of FMOS, putting emphasis on the prime focus unit consisting of the near-infrared corrector, the fibre positioner, the mechanical structure, and the IR spectrograph. The commissioning of the instrument is supposed to be at the end of 2004. The design goals and expected performances of the FMOS are summarized in Table 2.

Item	Specification	Notes
Prime Focus Corrector		
Field of view	$30'$	
Image size	RMS less than $0''.3$	
Focal plane	Flat	
F ratio	F/2	High-NA optical fibre
Telecentricity error	1.6 degree	At $15'$
Fibre Positioner		
No. of fibres	400	
Fibre core diameter	100 μm = $1''.2$	Optimized for faint galaxies
Couping efficiency to F/2	80 %	Worst case
Positioning accuracy	10 μm	With 5 iterations
Fibre configuration time	$<$ 10 min	
Fibre Connector		
Input F ratio	F/2	
Output F ratio	F/5	Minimize focal ratio degradation
Connector efficiency	$>$ 95 %	
OH-Suppression Spectrograph		
Input F ratio	F/5	
Slit length	120 mm	400 fibres
Wavelength coverage	0.9-1.8 μm	z, J, H - bands
Temperature Inside	-50 C°	Refrigerator
Spectral resolution modes		
	Low-resolution	High-resolution
Resolution	R = 500	R = 2200
Spectral Sampling	4 Å/ pixel	1 Å/ pixel
Camera		
Lens system	6 lens	Fused silica
Throughput	62 %	With AR coating
Detector	HAWAII 2	
Readout noise	$< 10\ e^-$	
Wavelength range	0.9-1.8 μm	Using thermal cut filter
Total		
Throughput model	13% at 1.2μm, 7% at 1.6μm	Low-resolution mode
	14% at 1.2μm, 9% at 1.6μm	High-resolution mode
Limiting magnitude	$z = 22.2, J = 22.1, H = 20.7$	Low-resolution mode
	$z = 21.4, J = 21.2, H = 20.4$	High-resolution mode

Table 2. Expected Performance of FMOS

ACKNOWLEDGMENTS

Authors would like to acknowledge contributions of Gabriella Frost, John Dawson, Roger Haynes, Ian Lewis, and Guy Woodhouse in promoting the FMOS project. The FMOS project in the definition phase of conceptual design has jointly been sponsored by NAO (Japan), PPARC (UK) and AAO.

REFERENCES

1. Iwamuro,F., Oya,S., Tsukamoto,H., and Maihara,T., 1996, ApJ, 466, L70-L73
2. Iwamuro,F., Motohara,K., Maihara,T., Hata,R., and Harashima,T., 2001, PASJ, 53 355
3. Gillingham,P., Miziarski,S., Akiyama,M., and Klocke,V., 2000 Proc. SPIE. **4008**, 1395
4. Gillingham,P., Brzeski,J., Dawson,J., Farrell,T., Frost,G., Griesbach,J., Haynes,R., Moore,A., Smedley,S., Smith,G., Waller,L, and Akiyama,M., 2002 proc. SPIE 4841, (in press.)
5. Komiyama,Y., et al. 2002 Proc. SPIE 4841 (in press.)
6. Lewis,I.J., Dalton,G.B., Tosh,I.A., Robertson,D.J., and Murray,G.J., 2002 Proc. SPIE 4841 (in press.)
7. Maihara,T., et al. 2000 Proc. SPIE. **4008**, 1111
8. Maihara, T., and Iwamuro, F. 2000 in Imaging the Universe in Three Dimensions: Astrophysics with Advanced Multi-Wavelength Imaging Devices (eds. W. van Breugel & J. Bland-Hawthorn), ASP Conf. Series,
9. Moore, A., Gillingham, P., Griesbach, J., and Akiyama, M., 2002 Proc. SPIE 4841 (in press.)
10. Motohara,K., Iwamuro,F., Maihara,T., Oya,S., Tsukamoto,H., Imanishi,M., Terada,H., Goto,M., Iwai,J., Tanabe,H., Hata,R., Taguchi,T., and Harasima,T., 2002 PASJ, 54, 315
11. Murray,G.J., Allington-Smith,J.R., Dipper,N.A., Luke,P., and Robertson,D.J., 2002 Proc. SPIE 4841 (in press.)